Magnetic Order Arising from Structural Distortion: Structure and Magnetic Properties of Ba_2LnMoO_6

Edmund J. Cussen,* Danny R. Lynham, and Joseph Rogers

The School of Chemistry, The University of Nottingham, Nottingham NG7 2RD, United Kingdom

Received January 30, 2006. Revised Manuscript Received April 5, 2006

The compounds Ba_2LnMoO_6 (Ln = Nd, Sm, Eu, Gd, Dy, Y, Er, and Yb) have been synthesized by solid-state techniques under reducing conditions at temperatures up to 1300 °C. Rietveld analyses of X-ray and neutron powder diffraction data show that these compounds adopt cation-ordered perovskite phases. At room temperature Ba_2NdMoO_6 and Ba_2SmMoO_6 adopt tetragonally distorted structures in the space groups *I*4/*m* and *I*4/*mmm*, respectively, while the data collected from all other compounds could be fitted in the cubic space group *Fm*3*m*. Bond valence sums show that the observed tetragonal distortions are driven by the bonding requirements of Ba^{2+}. Neutron powder diffraction data collected below T_N = 15(1) K show that Ba_2NdMoO_6 is triclinically distorted ($I\bar{1}$: a = 5.9790(2) Å, b = 5.9840(2) Å, c = 8.6024(2) Å, α = 89.854(2)°, β = 90.056(5)°, γ = 90.003(5)°) and that Nd^{3+} and Mo^{5+} are antiferromagnetically ordered. Magnetic susceptibility data show that this compound behaves as a Curie−Weiss paramagnet above this temperature, and no other compounds in the series show evidence of magnetic order down to 2 K. Ba_2YMoO_6 and Ba_2YbMoO_6 both remain entirely paramagnetic to 2 K due to perfect geometric frustration of the cubic lattice, indicating that next-nearest-neighbor interactions between like cations dominate over nearest-neighbor Mo−O−Ln exchange. The magnetic structure of Ba_2NdMoO_6 is rationalized with reference to the splitting of the t_{2g} manifold of Mo^{5+} by the Jahn−Teller distortion and the associated introduction of anisotropic magnetic superexchange.

Introduction

The perovskite family of compounds has been widely studied due to the large range of stoichiometries and hence chemistry which can be achieved in the structure and the exotic physical properties that result. The prototypical perovskite structure contains a larger cation in a 12-coordinate environment and a smaller cation, M, in octahedral coordination, with these MO_6 octahedra linked by shared vertexes giving rise to a continuous, cubic structure. It has long been recognized that this structure can undergo an enormous range of structural distortions[1] to accommodate large variation in relative cation sizes, and this variation can be further enhanced by a cation-ordered arrangement of large and small MO_6 units.[2] The stability of these structures arises because the mean size of the octahedral interstice is close to that of the ideal perovskite structure, although the individual cation size may show a large variation from this value.[3]

The study of such double perovskites has undergone a renaissance since the report of magnetoresistance in Sr_2FeMoO_6 at room temperature in modest magnetic fields.[4] The properties of Sr_2FeMoO_6 have been rationalized in terms of superexchange between Fe^{3+} and Mo^{5+}, leading to antiparallel alignment of differing magnetic moments, which leads to incomplete spin cancellation and ferrimagnetic order below 420 K. The potentially useful magnetoresistive effect arises due to the fully polarized electron density contributed from Mo^{5+} occupying a delocalized band while the electrons arising from Fe^{3+} are fully localized in a $t_{2g}^3e_g^2$ configuration. The related compound Ba_2FeMoO_6 shows similar behavior below a magnetic transition at 308 K;[5] the reduced temperature arises from the weakened exchange interaction and reduced orbital overlap due to the increased atomic separation associated with replacing Sr^{2+} with the larger Ba^{2+} cation. The potential applications of this behavior have led to an extensive study of related perovskite materials which contain a mixture of cations on the octahedral sites.[5−9]

The literature contains a number of related phases A_2LnMO_6 (A = Sr or Ba, Ln = lanthanide, M = transition metal). The study of these compounds permits subtle variations in the structure due to the large number of lanthanides and so provides an opportunity to examine in detail the interplay between structure and magnetic behavior in a large group of double perovskites. We have chosen to study the magnetic interactions in the family Ba_2LnMoO_6, which contains a mixture of Mo^{5+} and Ln^{3+} oxide octahedra. In these compounds the Mo^{5+} (t_{2g}^1) moment may couple with

* To whom correspondence should be addressed. E-mail: edmund.cussen@nottingham.ac.uk. Phone: +44 115 951 3503. Fax: +44 115 951 3563.

(1) Woodward, P. M. *Acta Crystallogr.* **1997**, *B53*, 32.
(2) Blasse, G. *Philips Res. Rep.* **1965**, *20*, 327.
(3) Battle, P. D.; Jones, C. W.; Studer, F. *J. Solid State Chem.* **1991**, *90*, 302.
(4) Kobayashi, K.-I.; Kimura, T.; Sawada, H.; Terakura, K.; Tokura, Y. *Nature* **1998**, *395*, 677.
(5) Ritter, C.; Ibarra, M. R.; Morellon, L.; Blasco, J.; Garcia, J.; De Teresa, J. M. *J. Phys.: Condens. Matter* **2000**, *12*, 8295.
(6) Viola, M. C.; Martinez-Lope, M. J.; Alonso, J. A.; Velasco, P.; Martinez, J. L.; Pedregosa, J. C.; Carbonio, R. E.; Fernandez-Diaz, M. T. *Chem. Mater.* **2002**, *14*, 812.
(7) Caspi, E. N.; Jorgensen, J. D.; Lobanov, M. V.; Greenblatt, M. *Phys. Rev. B* **2003**, *67*.
(8) Chan, T. S.; Liu, R. S.; Guo, G. Y.; Hu, S. F.; Lin, J. G.; Chen, J. M.; Attfield, J. P. *Chem. Mater.* **2003**, *15*, 425.
(9) Cussen, E. J.; Thomas, M. F. *J. Mater. Chem.* **2005**, *15*, 1084.

10.1021/cm0602388 CCC: $33.50
Published on Web 05/10/2006

the unpaired electrons in the 4f electrons of the Ln^{3+} cations. The 4f orbitals are too contracted to form appreciable orbital overlap with the 2p orbitals of the oxide ligands, so the empty 5d Ln orbitals are expected to mediate the magnetic exchange. Although no general observations have been made for the magnetic interactions of the lanthanides on the octahedral sites of the perovskite structure, it would be anticipated that the greater the orbital overlap between the M and oxide orbitals the stronger the magnetic exchange interaction. Here we present a series of compounds which show the opposite effect and show a correlation between structural distortion and magnetic ordering. This unexpected observation is the result of an uncommon Jahn−Teller distortion driven by the degenerate ground state of Mo^{5+}.

Experimental Section

Samples were synthesized using conventional solid-state techniques. Stoichiometric mixtures of $BaCO_3$, Ln_2O_3 (which was stored at 800 °C), and MoO_3 were intimately mixed and pressed into 13 mm pellets under a load of 1.5 t. These pellets were heated in air from 500 to 900 °C at a rate of 0.5 °C min^{-1} and held at this temperature for ca. 10 h. The pellets were then thoroughly ground, repelleted, and then heated at temperatures up to 1300 °C under a dynamic atmosphere of 5% H_2 in N_2. The samples were held at 1300 °C for several days before being cooled to room temperature, reground, and heated again. The progress of the reaction was monitored using X-ray powder diffraction, and the reaction was judged to be complete when the resultant X-ray pattern could be indexed as a single perovskite phase. In every case, the final heat treatment involved cooling the sample to room temperature under 5% H_2. This cooling process typically lasted 4 h.

X-ray powder diffraction data were collected using a Philips Xpert powder diffractometer operating with Cu Kα radiation in Bragg−Brentano geometry. Data were collected over the range $10° \leq 2\theta \leq 90°$ using a step size of $\Delta 2\theta = 0.02°$ from samples mounted on an aluminum slide. Neutron powder diffraction data were collected using both the constant-wavelength instrument D2b at the Institut-Laue Langevin, Grenoble, France, and the time-of-flight diffractometer Polaris at the ISIS facility at the Rutherford-Appleton Laboratories, Didcot, U.K. In both cases the samples were contained in cylindrical vanadium cans of internal diameters between 7 and 12 mm to give fill depths of 20−30 mm. The diffraction data were analyzed by Rietveld refinement[10] using the GSAS suite of programs.[11] The background was modeled using a shifted Chebyshev function. The Bragg peak shape for data collected at constant wavelength was modeled using a pseudo-Voigt function. In the case of neutron diffraction data collected using the Polaris instrument, the peak shape was modeled using a convolution of a pseudo-Voigt function and exponential functions to account for the energy profile of the incident neutron pulse. The magnetic form factor for Nd^{3+} was described using literature values.[12] No such information was available for Mo^{5+}, and the literature values for the form factor of Mn^{3+} were substituted, due to the similarity in ionic radii of the these two cations.

Magnetic measurements were carried out using a Quantum Design SQUID magnetometer. The samples were contained in gelatin capsules which were themselves mounted in straws which provided an invariant diamagnetic background that did not influence the SQUID detection coils. dc susceptibility measurements were carried out in applied fields of 100 and 1000 G after the sample was cooled in either zero applied field (zero-field-cooled, zfc) or the measuring field (field-cooled, fc). ac susceptibility data were collected in zero applied dc field with an ac field of amplitude 5 G operating at frequencies of 10, 100, and 1000 Hz.

Results

Room Temperature Structures. Preliminary assessment of the X-ray powder diffraction patterns obtained from the series Ba_2LnMoO_6 indicated that all of these phases adopt perovskite-related structures. The X-ray diffraction data collected from Ba_2NdMoO_6 showed evidence of peak splitting at a high angle, indicating a significant metric distortion from cubic symmetry. Due to the presence of so many strong scatterers, X-ray diffraction has a poor sensitivity to oxide anions in this compound, so neutron powder diffraction was employed to determine the structure of this compound. The neutron diffraction data collected from Ba_2NdMoO_6 at room temperature could be satisfactorily indexed using a tetragonally distorted perovskite structure with lattice parameters $a \approx a_p\sqrt{2}$ and $c \approx 2a_p$, where a_p is the lattice parameter for the simple cubic perovskite containing one AMO_3 formula unit in the unit cell. The tetragonal indexing is associated with chemical cation ordering between the B-site cations and is compatible with two types of distortion which possess space group symmetry of *I*4/*m* (No. 87) or *I*4/*mmm* (No. 139). These space groups share systematic absences, so the correct structural model can only be identified by comparing the quality of fit achieved in each space group. Both structural models constrain all metal cations to special positions, with zero degrees of translational freedom, and the difference between the two space groups lies in the oxide anion positions; in *I*4/*mmm* the oxide anions occupy 4e (0, 0, *z*) and 8h (*x*, *x*, 0), whereas in *I*4/*m* the latter has an additional degree of freedom, 8h (*x*, *y*, 0). Fitting neutron data in *I*4/*mmm* resulted in the fit parameter for the highest resolution neutron data $R_{wp} = 8.28$ and a fit which contained large intensity mismatches across the measured *d* spacing range. Fitting the data in the lower symmetry space group *I*4/*m* led to an immediate improvement in the quality of the fit ($R_{wp} = 1.67$). Refinement of the oxygen site fractional occupancies gave a value of unity, so the occupancies were subsequently fixed at this value. This model was refined to convergence against the X-ray and neutron diffraction data simultaneously, yielding the fit shown in Figure 1 and the fit parameters $R_{wp} = 3.00$ and $\chi^2 = 1.434$ for 48 variables including 2 lattice parameters, 3 positional parameters, and 7 displacement parameters. The derived atomic parameters are collected in Table 1.

Due to the high neutron absorption cross section of the lanthanides, the compounds containing Sm, Eu, Gd, and Dy were structurally characterized using X-ray powder diffraction. Ba_2SmMoO_6 showed peak splitting which resulted in clearly resolved peaks for $2\theta > 60°$. Comparison of the high angle range with the corresponding data collected from Ba_2NdMoO_6 shows that the magnitude of the metric distortion is significantly smaller in Ba_2SmMoO_6. Fitting these data

(10) Rietveld, H. M. *Acta Crystallogr.* **1969**, *2*, 65.
(11) Larson, A. C.; von Dreele, R. B. *General Structure Analysis System (GSAS)*; Los Alamos National Laboratories: Los Alamos, NM, 1990.
(12) Brown, P. J. *International Tables for Crystallography*, 4th ed.; Kluwer Academic Publishers: Dordrecht, The Netherlands, 1995; Vol. C, p 512.

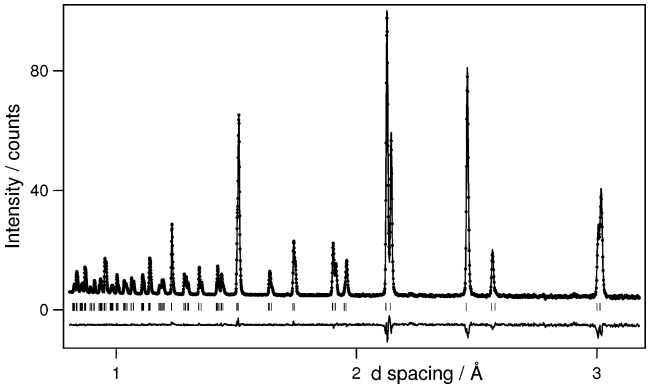

Figure 1. Observed (dots), calculated (line), and difference neutron powder diffraction patterns collected from Ba_2NdMoO_6 at room temperature.

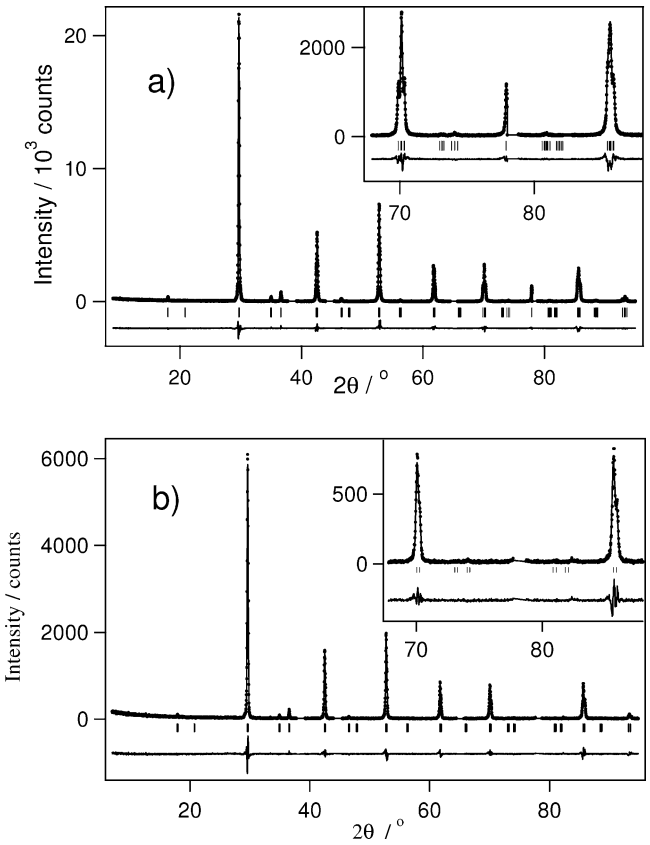

Figure 2. Observed (dots), calculated (line), and difference X-ray powder diffraction patterns collected from (a) Ba_2SmMoO_6 and (b) Ba_2EuMoO_6 at room temperature. Excluded regions were contaminated with peaks from the aluminum sample holder.

in *I*4/*m* resulted in a good level of agreement between the observed and calculated data ($R_{wp} = 11.10$, $R_p = 7.21$, $\chi^2 = 2.457$), but the refinement would not converge due to instability in the oxide ion positions. Most noticeably the oxide ion occupying the 8h site was close to the *x*, *x*, 0 position of the *I*4/*mmm* description, so this space group was

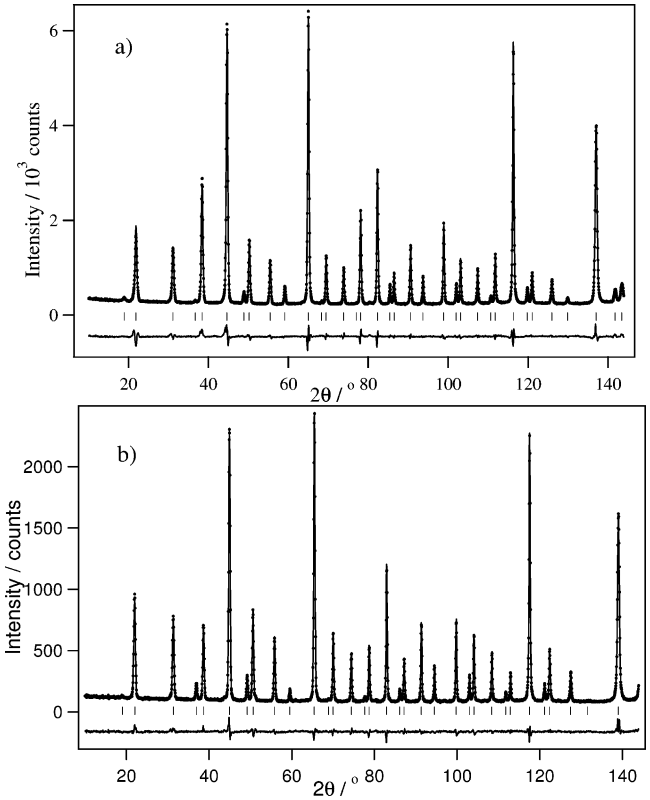

Figure 3. Observed (dots), calculated (line), and difference neutron powder diffraction patterns collected from (a) Ba_2YMoO_6 and (b) Ba_2YbMoO_6 at room temperature.

employed. This gave a nearly identical quality of fit and readily converged to give the fit as shown in Figure 2. We follow convention in assigning the higher space group where ambiguity exists, but note that the unavailability of neutron diffraction data means that this assignment should not be considered conclusive. X-ray powder diffraction data collected from Ba_2LnMoO_6 (Ln = Eu, Gd, Dy, Y, Er, Yb) showed no evidence of peak splitting and were fitted in the cubic space group $Fm\bar{3}m$ as shown in Figure 2 for Ba_2EuMoO_6. This space group assignment was confirmed by neutron diffraction data collected from Ba_2YMoO_6, Ba_2ErMoO_6, and Ba_2YbMoO_6 at room temperature. The availability of neutron diffraction data on these compounds permitted greater precision in the determination of the oxide ion positions, allowing anisotropic modeling of the oxide anion displacement parameters. The resultant fits are shown in Figure 3. Crystallographic disorder of the Ln^{3+} and Mo^{5+} cations over the two six-coordinate sites was permitted, but in every case this indicated that no detectable mixing had occurred, and the refined occupancies remained within 3 standard deviations of the ideally ordered values. Therefore, the fractional occupancies were fixed at the values associated with complete cation ordering. Similarly testing the oxide

Table 1. Atomic Parameters of Ba_2NdMoO_6 Derived from Rietveld Refinement against Neutron Diffraction Data Collected at Room Temperature[a]

atom	*x*	*y*	*z*	$100U_{11}$/Å^2	$100U_{22}$/Å^2	$100U_{33}$/Å^2	$100U_{12}$/Å^2
Ba	0	$^1/_2$	$^1/_4$	0.48(2)	0.48(2)	0.65(3)	
Mo	0	0	$^1/_2$	−0.02(3)	−0.02(3)	−0.09(4)	
Nd	0	0	0	0.12(2)	0.12(2)	−0.06(3)	
O(1)	0	0	0.26935(9)	1.77(3)	1.77(3)	0.27(4)	
O(2)	0.24228(9)	0.29916(9)	0	0.81(4)	1.02(3)	1.85(3)	−0.54(4)

[a] *I*4/*m*: $a = 6.01412(2)$ Å, $c = 8.57494(5)$ Å, $V = 620.304(4)$ Å^3.

Table 2. Fit Parameters and Selected Structural Data Derived for Ba_2LnMoO_6 at Room Temperature

Ln	space group	R_{wp}	R_p	χ^2	*a*/Å	*c*/Å	V^a/Å^3	Ln−O/Å	Mo−O/Å
Nd[b]	*I*4/*m*	2.29	3.64	1.376	6.01412(2)	8.57494(5)	620.304(4)	2.3152(6) × 4 2.3097(8) × 2	1.9778(8) × 4 1.9650(6) × 2
Sm[c]	*I*4/*mmm*	11.62	7.43	2.664	5.98954(6)	8.50030(12)	609.89(2)	2.28(2) × 4 2.253(12) × 2	1.983(12) × 4 1.97(2) × 2
Eu[c]	$Fm\bar{3}m$	16.20	11.47	1.861	8.46131(16)		605.78(4)	2. 271(14) × 6	1.960(14) × 6
Gd[c]	$Fm\bar{3}m$	13.20	9.27	2.443	8.44816(11)		602.96(3)	2.242(13) × 6	1.982(13) × 6
Dy[c]	$Fm\bar{3}m$	11.59	7.72	2.24	8.39982(12)		592.67(3)	2.257(10) × 6	1.943(10) × 6
Y[b]	$Fm\bar{3}m$	6.12	4.72	0.5166	8.39091(8)		590.78(2)	2.2294(8) × 6	1.9961(8) × 6
Er[b]	$Fm\bar{3}m$	6.13	4.83	1.592	8.37170(9)		586.73(2)	2.211(2) × 6	1.975(2) × 6
Yb[b]	$Fm\bar{3}m$	4.45	3.48	2.929	8.33780(8)		579.64(2)	2.1905(14) × 6	1.9785(14) × 6

[a] Volume occupied by four formula units [b] From Rietveld refinement against neutron powder diffraction data. [c] From Rietveld refinement against X-ray powder diffraction data.

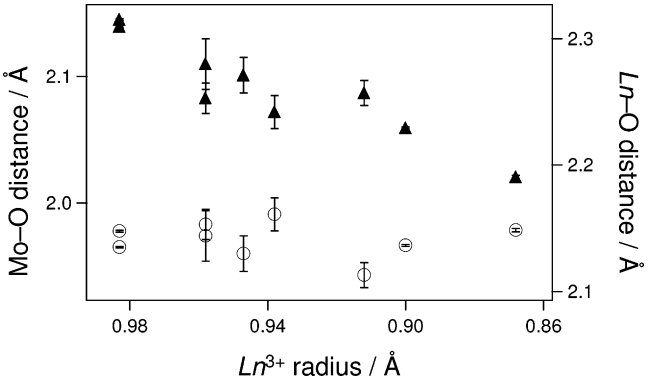

Figure 4. Variation in Ln−O (triangles) and Mo−O (circles) distances as a function of the ionic radius of Ln^{3+} in the series Ba_2LnMoO_6. Error bars indicate 1 standard deviation derived from the Rietveld refinements.

site occupancies showed that these compounds are fullystoichiometric in oxygen, so this variable was removed from the refinements.

The fit parameters and structural information derived from these Rietveld refinements are collected in Table 2. The Mo−O bond distance derived from these fits is largely invariant in these compounds, while the Ln−O distance(s) shows a variation which is in keeping with expectations from the ionic radii. The unit cell volume (normalized for four formula units) shows a linear relationship with the lanthanide radius. These structural parameters are collected in Figure 4. It is noteworthy that where anisotropic displacement parameters have been used the oxide ions show a largely spherical distribution of neutron scattering density.

Magnetic Measurements. The dc magnetization of these compounds was recorded as a function of temperature in applied fields of 100 and 1000 G. In every case the resulting magnetic susceptibilities were independent of the measuring field over the full temperature range studied, $2 \leq T/K \leq 300$. The data collected from Ba_2NdMoO_6 are shown in Figure 5. These data were fitted to the Curie−Weiss law in the temperature range $220 \leq T/K \leq 300$, with the results shown in Table 3. At 15(1) K both the zero-field-cooled and field-cooled data pass through a sharp maximum. The magnetic susceptibilities of all other compounds under discussion did not contain maxima or divergence between zfc and fc data over the whole temperature range studied. Data collected from Ba_2LnMoO_6 (Ln = Gd, Dy, Y, Er, Yb) were fitted to the Curie−Weiss law, with the resulting Curie and Weiss constants collected in Table 3. Due to the temperature dependence of the magnetic moments[13] of Sm^{3+} and Eu^{3+}, this approach was not suitable for the data collected from Ba_2SmMoO_6 and Ba_2EuMoO_6. Representative dc magnetic susceptibility data are shown in Figure 5. To further probe the nature of the magnetic transition in Ba_2NdMoO_6 and the properties of the other compounds, a series of ac susceptibility measurements were carried out.

The ac susceptibility data collected from Ba_2NdMoO_6 showed a maximum in the in-phase contribution at 14.5(5) K as shown in Figure 6. Below this temperature there is no frequency dependence to the susceptibility, indicating the absence of spin glass behavior below this temperature. ac susceptibility data collected from Ba_2LnMoO_6 (Ln = Dy, Er, Y, Yb) showed no frequency dependence and confirmed the Curie−Weiss paramagnetic behavior observed in the dc measurements. The data collected from Ba_2EuMoO_6 showed the same local maximum observed in the dc data. There was no frequency dependence observed in this compound, suggesting that all magnetic moments in this compound remain dynamic over the full temperature range studied.

Low-*T* Neutron Diffraction Measurements on Ba_2NdMnO_6. Neutron powder diffraction data were collected from Ba_2NdMoO_6 at 3.5 K to probe the nature of the magnetic transition at 15(1) K. These data could be modeled using a unit cell of approximately the same dimensions as the room temperature structure, but contained additional low-angle Bragg peaks which were systematically absent from the *I*4/*m* indexing. Data collected at 10 K showed that these low-angle peaks had reduced intensity, and they were absent from a third data set collected at 18 K as shown in Figure 7. This strong temperature dependence, and the absence of additional peaks at higher angle, indicates that these peaks are magnetic in origin and indicative of a magnetic unit cell of the same dimensions as the nuclear cell (i.e., $k = [000]$), but with reduced symmetry.

It was also evident that a degree of peak broadening had occurred at high diffraction angles. Such broadening is usually indicative of a structural distortion resulting in a crystal system of lower symmetry; i.e., an increased number of lattice parameters causes an increase in the number of allowed reflections. To test whether such a reduction in symmetry could model the observed peak broadening, we carried out a series of LeBail extractions in tetragonal (*P*4, No. 75), orthorhombic (*P*222, No. 16), and monoclinic (*P*2, No. 3) space groups with lattice parameters similar to those

(13) Kahn, O. *Molecular Magnetism*; VCH Publishers: New York, 1993.

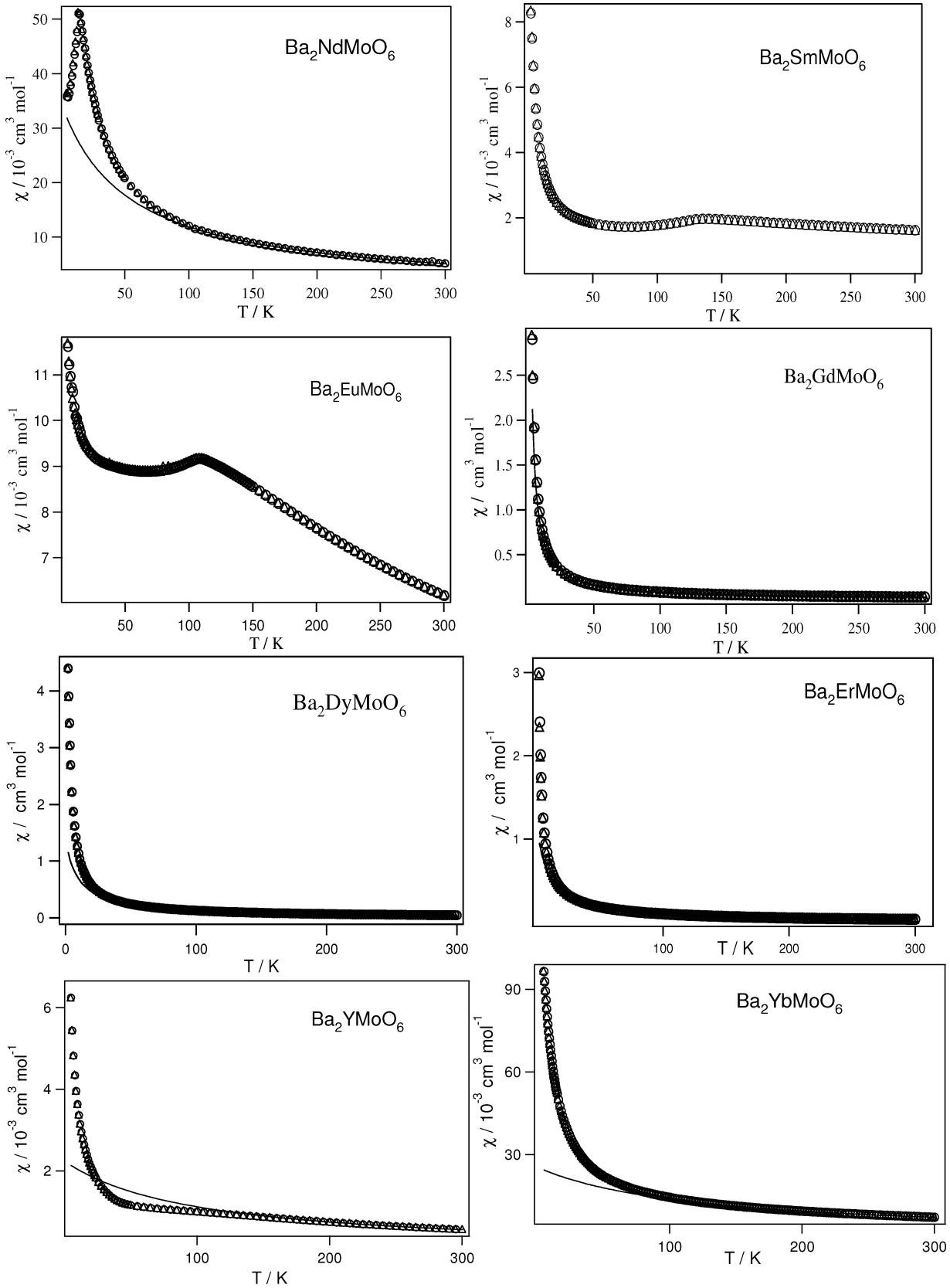

Figure 5. dc magnetic susceptibilities of Ba_2LnMoO_6 (Ln = Nd, Sm, Eu, Gd, Dy, Er, Y, Yb) collected after the sample was cooled in zero field (circles) and the measuring field of 1000 G (triangles). The solid lines represent Curie−Weiss fits in the range $220 \leq T/K \leq 300$.

observed at room temperature. This approach employs symmetry information and the dimensions of the unit cell and allows refinement of the calculated intensities of the Bragg peaks; i.e., it is independent of a structural model. While all of these fits satisfactorily indexed all of the observed peaks in the pattern, including those low-angle peaks of magnetic origin, the resultant indices of fit quality showed no appreciable improvement ($P4$ and $P2$ yield values of $R_{wp} = 3.37$ and 3.32, respectively) and failed to provide a good match to the observed broadening of peaks at high

Table 3. Parameters Derived from Fitting Magnetometry Data from Ba_2LnMoO_6 to the Curie−Weiss Law[a] in the Temperature Range $220 \leq T/K \leq 300$

compd	$C/(cm^3\ K\ mol^{-1})$	Θ/K	μ_{calcd}/μ_B[b]	μ/μ_B
Ba_2NdMoO_6	1.802(6)	−51.6(8)	4.01	3.80(4)
Ba_2GdMoO_6	8.063(7)	−0.4 (2)	8.13	8.03(2)
Ba_2DyMoO_6	13.80(5)	−10(1)	10.79	10.51(2)
Ba_2YMoO_6	0.225(1)	−91(1)	1.73	1.34(1)
Ba_2ErMoO_6	10.875(8)	−9.5(2)	9.73	9.33(1)
Ba_2YbMoO_6	2.95(3)	−116(4)	4.86	4.86(3)

[a] The temperature-dependent magnetic moment of Sm^{3+} and Eu^{3+}makes the Curie−Weiss law inappropriate for Ba_2SmMoO_6 and Ba_2EuMoO_6. [b] $\mu_{calcd} = (\mu_{Ln}^2 + \mu_{Mo}^2)^{1/2} = \{(g[J(J+1)]^{1/2})^2 + (2[S(S+1)]^{1/2})^2\}^{1/2}$.

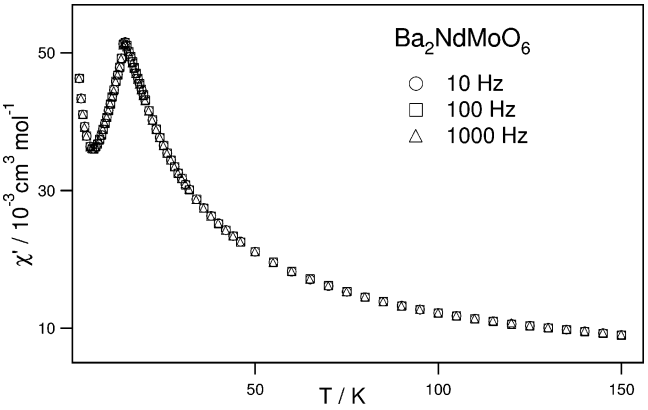

Figure 6. In-phase ac magnetic susceptibility of Ba_2NdMoO_6 collected at 10, 100, and 100 Hz in an applied ac field of 5 G.

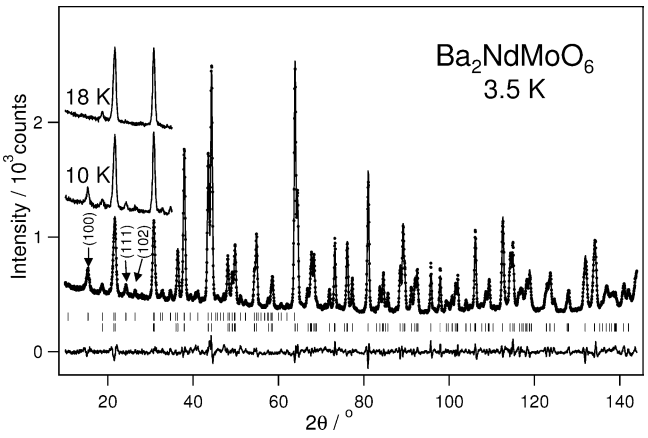

Figure 7. Observed (dots), calculated (line), and difference neutron powder diffraction data collected at 3.5 K from Ba_2NdMoO_6. The upper and lower sets of reflection markers indicate allowed Bragg peaks which are magnetic and nuclear in origin, respectively. Bragg reflections which are wholly magnetic in origin are indicated by arrows and indexed in a pseudotetragonal setting; e.g., (100) also includes (010). The inset shows the disappearance of the magnetic Bragg peaks on heating the sample to 18 K.

angle. A close examination of these fits showed that in many cases a broad peak shape had been employed to fit a single reflection to peaks which were clearly composed of multiple reflections. A group theoretical analysis[14] of the effect of structural distortions on the double perovskite structure has shown that additional octahedral tilting of the *I*4/*m* structure can lead to the adoption of triclinic space group $P\bar{1}$. This triclinic symmetry can be described in the nonstandard setting $I\bar{1}$, which conveniently uses the same setting as *I*4/*m*. Preliminary fits to the nuclear Bragg peaks showed that this

(14) Howard, C. J.; Kennedy, B. J.; Woodward, P. M. *Acta Crystallogr.* **2003**, *B59*, 463.

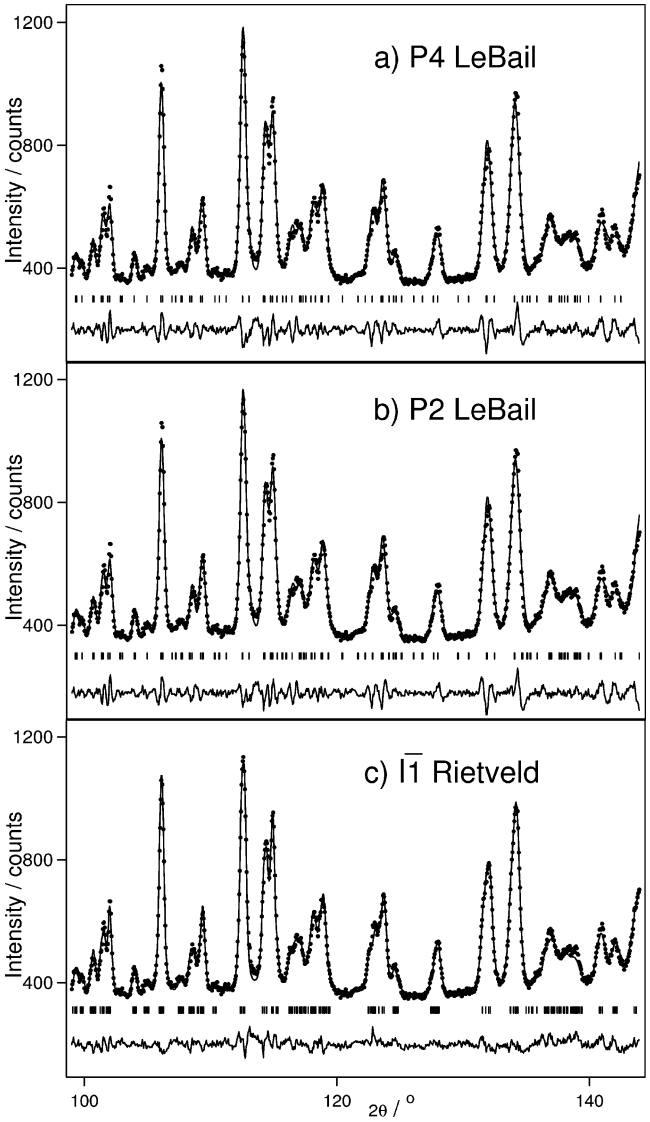

Figure 8. High-angle neutron powder diffraction data collected at 3.5 K showing the fits obtained using structureless refinements in (a) tetragonal and (b) monoclinic space groups. The improvement in fit using the triclinic space group $I\bar{1}$ even when constrained by the structural constraints of a Rietveld refinement is evident in (c).

provided a good fit to the broadened high-angle peaks. This improvement is such that the full structure Rietveld refinement resulted in a significantly better quality of fit than the structure-independent fit obtained using a monoclinic cell as shown in Figure 8. Therefore, we fitted the data collected from Ba_2NdMoO_6 in $I\bar{1}$ and a magnetic model in which the two Nd^{3+} and two Mo^{5+} cations contained in the unit cell formed antiferromagnetically coupled pairs to lead to complete spin cancellation, as indicated by the bulk magnetic susceptibility.

A magnetic unit cell containing two Nd^{3+} and two Mo^{5+} cations and zero net magnetization necessarily requires a magnetic structure in which the moments of the Nd cations on the corners of the unit cell are arranged antiparallel to the Nd occupying the body center and the Mo moments are constrained in the same way, although not necessarily collinear to Nd^{3+}. This could be described as containing Nd^{3+} (or Mo^{5+}) ferromagnetically coupled layers in the *xy* plane which are stacked antiferromagnetically along the *z* direction

Table 4. Bond Valence Sum Calculations for Ba in Room Temperature Ba_2LnMoO_6 Structures[a]

		Ba−O(1)/Å	BV1	Ba−O(2)/Å	BV2	Ba−O(3)/Å	BV3	BVS
Ba_2NdMoO_6	$I4/m$	2.8559(4)	0.230	3.01147(4)	0.153	3.2042(4)	0.092	1.88
Ba_2NdMoO_6	*$Fm\bar{3}m$*	*3.0330*	*0.144*					*1.73*
Ba_2SmMoO_6	$I4/mmm$	2.9986(10)	0.158	3.0031(5)	0.156			1.88
Ba_2SmMoO_6	*$Fm\bar{3}m$*	*3.0015*	*0.157*					*1.88*
Ba_2EuMoO_6	$Fm\bar{3}m$	2.9956(7)	0.159					1.91
Ba_2GdMoO_6	$Fm\bar{3}m$	2.9893(5)	0.162					1.94
Ba_2DyMoO_6	$Fm\bar{3}m$	2.9739(5)	0.169					2.03
Ba_2YMoO_6	$Fm\bar{3}m$	2.96955(4)	0.171					2.05
Ba_2ErMoO_6	$Fm\bar{3}m$	2.962505(3)	0.174					2.09
Ba_2YbMoO_6	$Fm\bar{3}m$	2.94978(6)	0.180					2.16

[a] Structures shown in italics are theoretical crystal structures with cubic symmetry exhibiting the same Ln−O and Mo−O distances as in the observed, tetragonal, structures.

without imposing any coupling between the Nd^{3+} and Mo^{5+} substructures. Initial refinements employed an antiparallel-moment of Nd that could be aligned in any direction in the cell. The moment of Mo was similarly refined, giving a total of six magnetic variables in the refinement. Due to the small number of magnetic Bragg peaks, this resulted in a highly unstable refinement due to large correlation between the different components of the magnetic moment as well as a correlation between the moments of Mo and Nd. While this led to a reasonable quality of fit and showed that the data could be fitted using a model in which the moment of Nd (2.5(2) μ_B) had components 0.2(2), 0.06(5), and 2.52(8) μ_B and the moment of Mo (0.7(2) μ_B) had components 0.3(10), −0.6(5), and 0.15(8) μ_B along the *x*, *y*, and *z* directions, it clearly indicated the high level of correlation between the different components of the magnetic moment. To reduce this correlation in the refinement, a number of magnetic models were tested which allowed the magnetic moments to align along the *x*, *y*, or *z* direction of the unit cell with the Nd and Mo moments constrained to be collinear. Alignment of the moments along the *z* direction resulted in a uniquely stable refinement with refined values of the magnetic moments of 2.46(5) and 0.16(4) μ_B for Nd and Mo, respectively. As illustrated in Figure 9 the magnetic unit cell has the same dimensions as the nuclear cell and the structure is composed of ferrimagnetic layers stacked antiferromagnetically along the *z* direction of the unit cell. The quality of this fit was identical to that obtained by the unconstrained refinement. Attempts to refine anisotropic displacement parameters failed to yield any improvement in the quality of the fit, indicating that these data are insensitive to such a detailed description of the atomic displacements. Anisotropic displacement parameters destabilized the refinement, so the atomic displacements were modeled isotropically. The final fit obtained to the 3.5 K data is shown in Figure 7 and yielded the fit parameters $R_{wp} = 3.14$ and $\chi^2 = 0.5252$. Although the derived moment of Mo is small, a trial model employing antiferromagnetic stacking of ferromagnetic sheets degraded the quality of the fit ($R_{wp} = 3.70$), and thus, the refinement clearly indicated antiparallel arrangements of Nd and Mo moments within the *xy* layers. It is quite possible that this magnetic structure represents a simplification of the actual magnetic phase; however, the correlation observed in these refinements indicates that these neutron powder diffraction data are unable to define additional variables in the magnetic structure. It is likely that the small value of the Mo^{5+} moment is an outcome of this simplification, but nevertheless, the ordering of the *z* components of Nd^{3+} and Mo^{5+} in the final magnetic model is clearly defined by these neutron diffraction data. The atomic coordinates are collected in Table 5, and the derived bond lengths and angles are listed in Table 6.

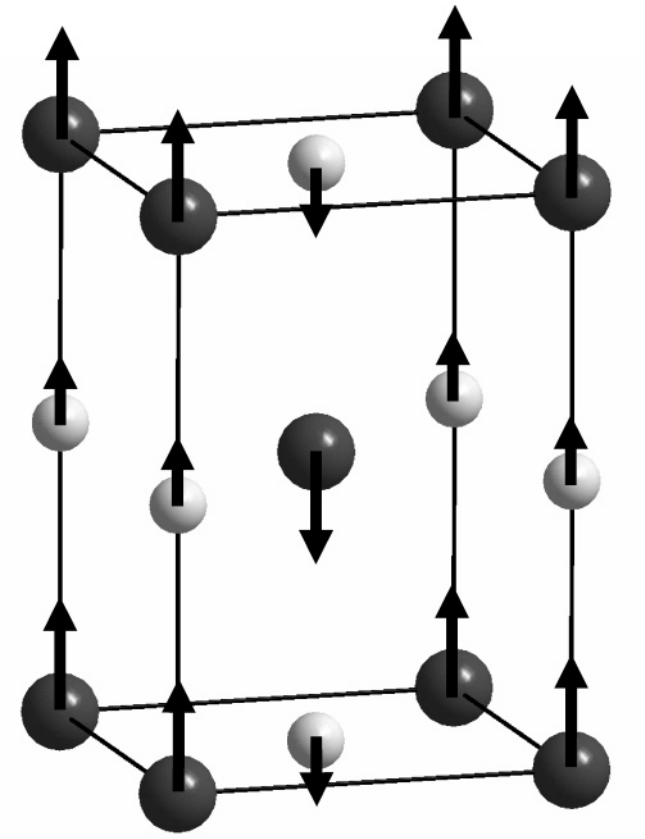

Figure 9. Magnetic structure of Ba_2NdMoO_6. Mo and Nd cations are shown as light gray and dark gray spheres, respectively, and all other atoms are omitted for clarity. The nuclear and magnetic structures have unit cells of the same dimensions.

Table 5. Atomic Parameters of Ba_2NdMoO_6 Derived from Rietveld Refinement against Neutron Diffraction Data Collected at 3.5 K[a]

atom	*x*	*y*	*z*	$100U_{iso}/Å^2$
Ba	−0.0044(12)	0.496(2)	0.2573(6)	0.24(4)
Mo	0	0	1/2	0.38(3)
Nd	0	0	0	0.38(3)
O(1)	0.002(3)	0.004(1)	0.2649(3)	1.22(5)
O(2)	0.2322(12)	0.3112(12)	0.0041(6)	1.31(13)
O(3)	0.6925(10)	0.2358(12)	−0.0027(8)	0.6(1)

[a] $I\bar{1}$: $a = 5.9790(2)$ Å, $b = 5.9840(2)$ Å, $c = 8.6024(2)$ Å, $\alpha = 89.854(2)°$, $\beta = 90.056(5)°$, $\gamma = 90.003(5)°$, $V = 307.783(11)$ Å^3.

Neutron diffraction data collected at 10 K were analyzed in a similar manner, yielding an ordered magnetic moment

Table 6. Selected Bond Lengths (Å) and Angles (deg) for Ba_2NdMoO_6 at 3.5 K

Ba−O(1)	2.943(13)	Mo−O(1)	2.023(3) × 2
Ba−O(1)	2.98(2)	Mo−O(2)	1.959(8) × 2
Ba−O(1)	3.01(2)	Mo−O(3)	1.956(7) × 2
Ba−O(1)	3.043(13)	Nd−O(1)	2.279(3) × 2
Ba−O(2)	2.827(9)	Nd−O(2)	2.323(8) × 2
Ba−O(2)	2.868(10)	Nd−O(3)	2.318(7) × 2
Ba−O(2)	3.196(11)		
Ba−O(2)	3.275(8)	O(1)−Mo−O(2)	88.2(5)
Ba−O(3)	2.764(10)	O(1)−Mo−O(3)	89.5(3)
Ba−O(3)	2.777(8)	O(2)−Mo−O(3)	89.1(4)
Ba−O(3)	3.275(8)	O(1)−Mo−O(1)	180
Ba−O(3)	3.292(11)	O(1)−Nd−O(2)	88.3(4)
		O(1)−Nd−O(3)	89.7(3)
Mo−O(1)−Nd	178.4(8)	O(2)−Nd−O(1)	89.2(3)
Mo−O(2)−Nd	161.8(4)	O(1)−Nd−O(1)	180
Mo−O(3)−Nd	163.5(3)		

of 2.07(5) μ_B per Nd and 0.17(5) μ_B per Mo. Data collected at 18 and 32 K were successfully fitted using a model in which there was no magnetic contribution to the Bragg scattering. In every case, attempts to fit the data in higher symmetry space groups failed to describe the peak shape at high angle. The lattice parameters from these fits are shown in Figure 10, and the Nd−O and Mo−O bond lengths derived from these refinements are compared with the room temperature values in Figure 11.

Discussion

Room Temperature Structures. Rietveld refinement against X-ray or neutron powder diffraction has shown that the compounds Ba_2LnMoO_6 adopt cation-ordered perovskites which are cubic for lanthanides smaller than Sm^{3+} and tetragonally distorted for Ln = Nd and Sm at room temperature. This agrees with the indexing previously carried out[15] on these compounds and provides the first structural description of these phases. The distortion observed for the larger lanthanides is driven by size mismatch, and this can be quantified using bond valence sums. If Ba_2NdMoO_6 and Ba_2SmMoO_6 formed cubic structures, while maintaining the same mean Ln−O (2.313 and 2.261 Å) and Mo−O (1.969 and 1.979 Å) distances as observed in the tetragonally distorted phases, the Ba^{2+} cations would be coordinated to 12 oxide ions at distances of 3.033 and 3.002 Å, respectively. The results of bond valence calculations on these hypothetical structures are collected in Table 4 and compared with the experimentally determined bond distances for the complete series of compounds. From inspection of these values it is clear that the structural distortion in Ba_2NdMoO_6 is driven by the bonding requirements of Ba.

Neutron diffraction studies[5] of the phases A_2FeMoO_6 (A = Ca, Sr, Ba) determined a typical Mo−O distance of ca. 1.97 Å which was independent of the A-site cation size. This distance was found in Ba_2LnMoO_6, which provides confirmation of the largely Mo^{5+} nature of molybdenum in A_2FeMoO_6. The Ln−O bond distances show no evidence for anomalous structural adjustments across the series and demonstrate the expected contraction with increasing atomic number. Examination of the anisotropic displacement parameters of the oxide anions in these materials shows a mostly isotropic arrangement of scattering density which is typical of a well-ordered perovskite phase; i.e., there is no evidence of uncommon dynamic or static disorder in the oxide positions.

The structural data collected from all of these phases show the presence of molybdenum in the expected pentavalent state. Assuming complete quenching of the orbital contribution to the Mo^{5+} moment, this cation contributes 1.73 μ_B to the magnetic susceptibility of these phases. Due to the large magnetic moments associated with some of the lanthanides in this study (Gd^{3+}, Dy^{3+}, and Er^{3+} contribute 7.94, 10.65,

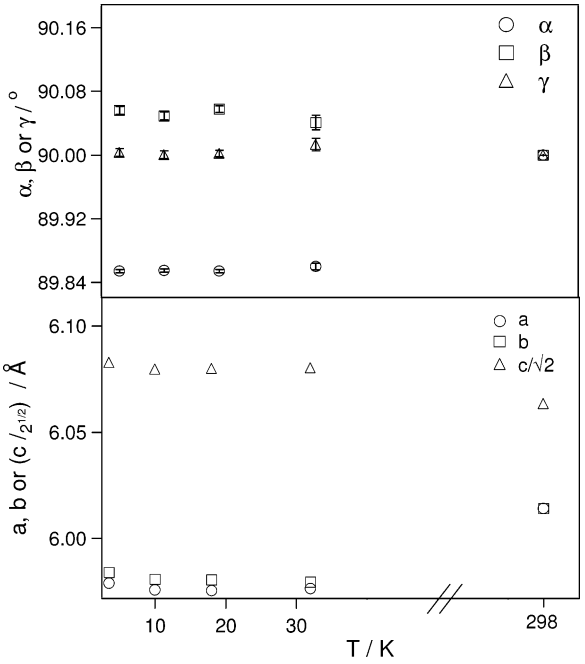

Figure 10. Variation in the lattice parameters of Ba_2NdMoO_6 as a function of temperature. For ease of comparison with the *a* and *b* parameters the values for the *c* axis are reported as $c/\sqrt{2}$. The standard deviations in *a*, *b*, and *c* are smaller than the symbols used.

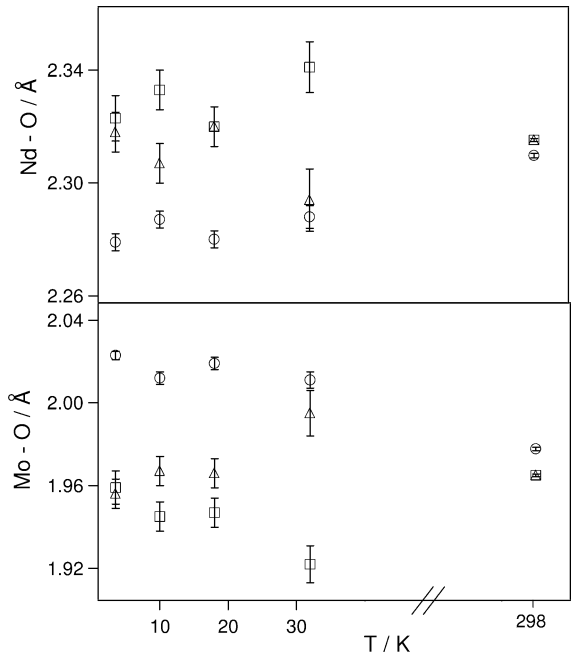

Figure 11. Variation of Nd−O (upper) Mo−O (lower) distances as a function of temperature. The error bars indicate 1 standard deviation derived from the Rietveld refinement.

(15) Brandle, C. D.; Steinfink, H. *Inorg. Chem.* **1971**, *10*, 922.

and 9.58 μ_B, respectively), it is not possible to conclude with certainty that Mo^{5+} is paramagnetic in these compounds. However, the absence of a maximum or history dependence in the dc susceptibility data and the independence of frequency in the ac susceptibility data suggest that all magnetic moments are dynamic at all temperatures down to 2 K. In these compounds there is good agreement between the paramagnetic moment derived from the Curie−Weiss fit to the dc magnetic susceptibility data and the expected moment, and this provides conclusive evidence that the Ln^{3+} moments are paramagnetic over the full temperature range studied.

Magnetic Measurements. The compounds Ba_2SmMoO_6 and Ba_2EuMoO_6 contain Ln^{3+} species which show temperature-dependent magnetic moments and thus are expected to lead to more complex paramagnetic behavior than the other compounds in this series. The magnetic susceptibility data collected from Ba_2SmMoO_6 and Ba_2EuMoO_6 are qualitatively similar to those reported[16] for Ba_2SmReO_6 and Ba_2EuReO_6 showing the susceptibility increasing at temperatures below a plateau at temperatures around 80 K. Attempts to fit the susceptibility data from Ba_2SmMoO_6 and Ba_2EuMoO_6 to Curie law expressions combining the temperature-dependent magnetic moment[13] of the lanthanide and the spin-only description of the Mo^{5+} susceptibility failed to provide a satisfactory fit to the data. Nevertheless, the absence of divergence between field-cooled and zero-field-cooled data suggests that neither the Ln^{3+} nor Mo^{5+} cations undergo magnetic ordering in the temperature range studied, although, as for Ln = Gd, Dy, and Er, this conclusion remains tentative. Due to the uncertainties in the magnetic behavior of Mo^{5+} in the above compounds, the discussion of magnetic properties will focus on the compounds where the magnetic contributions of Ln^{3+} and Mo^{5+} can be readily decoupled, namely, Ba_2NdMoO_6, Ba_2YMoO_6, and Ba_2YbMoO_6.

The magnetic behavior of Ba_2YMoO_6 is highly informative as this compound contains only a single paramagnetic species. The susceptibility data collected from this compound show a large negative Weiss constant, −91(1) K, and reasonable agreement between the observed and calculated paramagnetic moments. The Weiss constant indicates the presence of strong antiferromagnetic interactions in this compound, and as there is no evidence of chemical or structural disorder in this compound, these interactions would be anticipated to result in the formation of an antiferromagnetically ordered phase at a temperature of several tens of kelvin. However, no magnetic transition is observed down to 2 K. An understanding of these magnetic properties requires detailed consideration of the arrangement of the Mo^{5+} cations. These cations are in a cubic close-packed arrangement that results in each cation having 12 nearest neighbors at a distance of 5.933 Å. This arrangement can be considered to be constructed from edge-sharing tetrahedra of Mo^{5+}, giving rise to a triangular arrangement of magnetic interactions. It is not possible for a collinear arrangement of antiparallel magnetic moments to satisfy the interactions with all neighbors[17] within such an arrangement. This combination of triangular connectivity and antiferromagnetic coupling leads to perfect magnetic frustration, inhibiting the formation of a magnetically ordered phase, and thus, Ba_2YMoO_6 remains paramagnetic to 2 K.

The Curie−Weiss law provides a good fit to the susceptibility of Ba_2YbMoO_6 and shows excellent agreement between the observed paramagnetic moment, 4.86(3) μ_B, and that expected, 4.86 μ_B, to result from a full orbital contribution from Yb^{3+} and a spin-only magnetic moment of Mo^{5+}. The antiferromagnetic interactions indicated by the Weiss constant, −116(4) K, are more complex than those of Ba_2YMoO_6 due the presence of paramagnetic species on both of the octahedral sites in the lattice. If the magnetic properties were determined purely by antiferromagnetic superexchange between neighboring Mo^{5+} and Yb^{3+} cations, a ferrimagnetic phase would result in which all Yb^{3+} moments were aligned parallel to one another and antiparallel to all Mo^{5+} moments. Such a situation is found in Sr_2FeMoO_6, giving rise to ferrimagnetism below ca. 420 K, but in Ba_2YbMoO_6 the magnetic interactions involving Yb^{3+} are anticipated to be considerably weaker than those involving Fe^{3+}. An alternative situation could arise if the dominant magnetic interaction in Ba_2YbMoO_6 was the next-nearest-neighbor interaction Mo−O−O−Mo. In this case the magnetic interaction would be perfectly frustrated, as discussed for Ba_2YMoO_6, and a magnetically ordered phase would not be formed. The absence of a magnetic transition in Ba_2YbMoO_6 despite the presence of the strong antiferromagnetic interactions indicated by the Weiss constant may indicate that this next-nearest exchange is dominant, although the observations discussed below in Ba_2NdMoO_6 suggest that this is an overly simplistic description of the magnetic system.

Low-*T* Properties of Ba_2NdMoO_6. The neutron diffraction data show that Ba_2NdMoO_6 adopts a triclinically distorted structure collected in the temperature range $3.5 \leq T/K \leq 32$. We have not determined if this structural distortion involves a direct transition from $I4/m$ to $I\bar{1}$ or proceeds via an intermediate tilting scheme, such as $P2_1/n$, and we have not observed the temperature at which these transitions occur. Ba_2LaRuO_6 exhibits a similar triclinic distortion at room temperature,[18] although recent work[19] has used X-ray diffraction to examine this phase and suggested that this assignment may be doubtful. The original space group assignment was based on structural refinement against neutron diffraction data, and as for Ba_2NdMoO_6, the departure from higher metric symmetry was not large. Our confidence in the triclinic structure of Ba_2NdMoO_6 does not arise from the departure of the lattice parameters from those of a higher crystal system but rather from the substantial improvement in the fit to the observed data. The unfortunately named cubic perovskite family is famous for the large number of ways[1,14,20] in which the oxide octahedra tilt, and these distortions often have negligible impact on the positions

(16) Sasaki, Y.; Doi, Y.; Hinatsu, Y. *J. Mater. Chem.* **2002**, *12*, 2361.
(17) Harrison, A. *J. Phys.: Condens. Matter* **2004**, *16*, S553.
(18) Battle, P. D.; Goodenough, J. B.; Price, R. *J. Solid State Chem.* **1983**, *46*, 234.
(19) Fu, W. T.; IJdo, D. J. W. *Solid State Commun.* **2005**, *136*, 456.
(20) Woodward, P. M. *Acta Crystallogr.* **1997**, *B53*, 44.

of the cations that usually dominate the X-ray diffraction data. In the case of Ba_2NdMoO_6, and also of Ba_2LaRuO_6, the structural distortion is mainly exhibited by the oxide positions, so profile analysis of neutron diffraction data is vital if the symmetry is to be accurately determined. Neutron diffraction data show that the triclinic distortion in Ba_2NdMoO_6 exists up to at least 32 K. Over the temperature range $3.5 \leq T/K \leq 32$ we do not observe any significant variation in Mo−O/Nd−O distances or evidence of magnetostriction in the lattice parameters.

Our experiments show that Ba_2NdMoO_6 distorts and undergoes a substantial rearrangement on cooling from room temperature; the apical bonds undergo a large extension to 2.023(3) Å, while those in the plane contract to 1.956(7) and 1.959(8) Å. The NdO_6 octahedra show the anticipated thermal contraction on cooling. By neglecting the nonorthogonality of the *a*, *b*, and *c* lattice parameters and taking the mean value (5.9815 Å) of *a* and *b* at 3.5 K, the unit cell dimensions can be readily compared with those observed at room temperature. These show that the geometric changes in the coordination of Mo lead to an increase in the *c* lattice parameter of 0.0275(3) Å (0.320(3)%) on cooling from room temperature, which can be contrasted with the decrease in the *a* parameter of 0.0326(4) Å (0.542(6)%) observed over the same temperature range.

In ideal octahedral geometry the Mo^{5+} cation has the same triply degenerate ground state, $t_{2g}^1e_g^0$, as Ti^{3+}. $NaTiO_2$ contains TiO_6 octahedra and undergoes a structural transition at 250 K which is driven by a Jahn−Teller distortion of the Ti^{3+} environment.[21] At 5 K $NaTiO_2$ exhibits a distortion of the TiO_6 octahedra with two long (2.1153(6) Å) and four short (2.0609(6) Å) bonds. This distortion splits the t_{2g} manifold into three, singly degenerate states due to the reduction in site symmetry to 2/*m* (C_{2h}). The site symmetry of Mo in the triclinic structure *i* (C_i) permits angular distortion of the MoO_6 octahedra and eliminates the double degeneracy of d_{xz} and d_{yz} that exists at room temperature. Moreover, the magnitude of the distortion in bond lengths in $NaTiO_2$ provides an excellent match with that observed in Ba_2NdMoO_6 and suggests that the negative thermal expansion manifested in the *c* parameter of Ba_2NdMoO_6 is due to a Jahn−Teller distortion arising from the doubly (pseudo triply) degenerate ground state of Mo^{5+} observed at room temperature. Due to the low site symmetry of the oxide ion, the standard deviations associated with the MoO_6 angles are relatively large compared to the small observed angular deviations. As a consequence of this we are unable to determine reliably the relative energies of the d_{xz} and d_{yz} orbitals.

In addition to the static, ordered, Jahn−Teller distortions observed in the crystallographic bond lengths, it is possible that dynamic Jahn−Teller distortions occur in this structure. Such distortions are not propagated through the lattice and so do not effect the observed bond lengths, but can play a key role in determining the magnetic behavior.[22] These distortions contribute to positional disorder in the ligands and so would be manifested in the displacement parameters of the oxide ions in Ba_2NdMoO_6. However, our data showed no evidence of highly anisotropic displacements from the oxide ion positions. We note that all other compounds showed largely isotropic oxide ion displacement parameters and that the cubic symmetry observed for most phases indicates the presence of oxide octahedra which are perfectly regular on the time and dimension scales of a neutron diffraction experiment. We can conclude that Ba_2NdMoO_6 is the only compound which shows any structural evidence of Jahn−Teller instability.

The dc magnetic susceptibility data collected from Ba_2NdMoO_6 clearly show a magnetic transition at 15(1) K which leads to partial cancellation of magnetic moment, suggesting, although not proving, the formation of an antiferromagnetically ordered phase at this temperature. Above this temperature the magnetic susceptibility shows Curie−Weiss law behavior yielding a value for the Curie constant of 1.802(6) $cm^3\ K\ mol^{-1}$, which agrees reasonably well with that expected, 2.01 $cm^3\ K\ mol^{-1}$, on the basis of a spin-only contribution from Mo^{5+} and the free ion contribution from Nd^{3+}, $^4I_{9/2}$. We note that the observed value is significantly larger than that, 1.64 $cm^3\ K\ mol^{-1}$, which would result from the moment of Nd^{3+}, 3.62 μ_B, alone. From this we conclude that Mo^{5+} and Nd^{3+} undergo a simultaneous magnetic transition at 15(1) K and that both cations are paramagnetic above this temperature. It could be anticipated that the different strengths of magnetic exchange involving Mo and Nd would lead to different ordering temperatures for the two cation sublattices. However, observations of the related, monoclinically distorted phases Sr_2TbRuO_6, Sr_2HoRuO_6, and Ba_2PrRuO_6 have shown[23,24] that the d-metal and lanthanide sublattices undergo simultaneous magnetic transitions in these systems.

ac susceptibility measurements on Ba_2NdMoO_6 reproduce the maximum observed in the dc measurements and show no frequency dependence below the 15(1) K transition. The decrease in susceptibility clearly indicates a partial cancellation of magnetic moment, i.e., the formation of domains of antiferromagnetically coupled moments within the material. The absence of frequency dependence in the low temperature regime clearly shows that these domains are sufficiently large that the relaxation time is infinite compared to the applied frequencies. This is the signature of an antiferromagnetically ordered phase and indicates the absence of spin glass behavior. Due to the differing magnetic moments of Mo and Nd, the observed reduction in magnetic moment must be associated with antiparallel coupling between Nd−Nd and Mo−Mo pairs rather than the ferrimagnetism which would result from antiferromagnetic coupling between Nd−Mo nearest neighbors. The observation of magnetic Bragg peaks in the neutron diffraction data

(21) Clarke, S. J.; Fowkes, A. J.; Harrison, A.; Ibberson, R. M.; Rosseinsky, M. J. *Chem. Mater.* **1998**, *10*, 372.

(22) Cussen, E. J.; Rosseinsky, M. J.; Battle, P. D.; Burley, J. C.; Spring, L. E.; Vente, J. F.; Blundell, S. J.; Coldea, A. I.; Singleton, J. *J. Am. Chem. Soc.* **2001**, *123*, 1111.

(23) Parkinson, N. G.; Hatton, P. D.; Howard, J. A. K.; Ritter, C.; Ibberson, R. M.; Wu, M.-K. *J. Phys.: Condens. Matter* **2004**, *16*, 7611.

(24) Parkinson, N. G.; Hatton, P. D.; Howard, J. A. K.; Giblin, S. R.; Terry, I.; Ritter, C.; Mok, B. H.; Wu, M. K. *J. Mater. Chem.* **2005**, *15*, 1375.

collected at 3.5 and 10 K, but not 18 K, proves that Ba_2NdMoO_6 is an antiferromagnet below the magnetic transition observed in the susceptibility, $T_N = 15$ K. The adopted magnetic structure shows that the coupling between paramagnetic cations is anisotropic. Within the *xy* layers the Nd moments are coupled antiferromagnetically to neighboring Mo cations, leading to a ferrimagnetic layer with all Nd parallel to each other and antiparallel to Mo. The coupling along the *z* direction between Nd and Mo is ferromagnetic, leading to an antiferromagnetic stacking of layers.

The Nd−O−Mo exchange path along the *z* direction is constrained to 180° by symmetry at room temperature. On cooling, the structure distorts, and this angle is reduced to 178.4(8)° at 3.5 K. Nevertheless, the orbital overlap along the *z* direction is considerable when compared to the overlap in the *xy* plane, where the Nd−O−Mo angles are 161.8(4)° and 163.5(3)°. This deviation from linearity reduces the strength of magnetic exchange and could therefore be assumed to lead to the dominant interaction being manifested in the *z* direction while the *xy* magnetic arrangement was subordinate to this. The Weiss constant indicates that antiferromagnetic coupling occurs in this material, and it could therefore be anticipated that Nd^{3+} and Mo^{5+} would be coupled in an antiparallel fashion along the *z* direction, rather than show the observed parallel alignment. Clearly, an understanding of the magnetic interactions requires a more detailed examination of the various mechanisms for superexchange and the impact of the observed structural distortion on them.

Superexchange in metal oxides is mediated by the bridging oxide anions and can be considered to be dominated by a mixture of correlation and delocalization interactions. The former arises from simultaneous bond formation between the oxide ion and both cations, while the latter describes the transfer of an electron from one cation to the other and varies with the fourth power of orbital overlap.[25] Correlation superexchange between two cations each containing empty orbitals would lead to an antiparallel spin alignment, while the interaction between a half-filled orbital and an empty orbital would favor parallel alignment. Delocalization exchange cannot occur between empty orbitals, and the interaction between a half-filled orbital and an empty orbital would favor parallel alignment. We therefore see that the two mechanisms tend to reinforce one another but that exchange involving a nonspherical electronic arrangement can lead to conflicting interactions.

Consideration of these interactions in Ba_2NdMoO_6 indicates that the σ exchange involving the empty e_g orbitals of both Mo and Nd favors an antiparallel arrangement of moments while the π exchange would be between the partially occupied t_{2g}^1 orbitals of Mo and the empty t_{2g} orbitals of Nd. However, neither Nd^{3+} nor Mo^{5+} occupies geometrically perfect oxide octahedra, and a detailed examination of the cation coordination environment is necessary. At room temperature the tetragonal distortion shows a small difference in Mo−O distances between those in the plane, 1.9646(6) Å, and the apical bonds, 1.9771(9) Å. The electronic properties of a compound showing such a small distortion would typically be rationalized by treating the system as octahedral, i.e., containing a triply degenerate and doubly degenerate arrangement of d orbitals.

The Jahn−Teller-driven structural distortion observed on cooling eliminates this degeneracy. It has been argued that the angular distortion observed in $NaTiO_2$ (O−Ti−O = 94.2° at room temperature) introduces a splitting of ca. 0.4 eV. This distortion is considerably greater than that observed in Ba_2NdMoO_6 at 3.5 K, although, due to the uncertainties in bond angles, it is not possible to calculate the splitting in Ba_2NdMoO_6 with precision. Although we have not been able to determine the relative energies of Mo d_{xz} and d_{yz} orbitals, the small angular deviation in the MoO_6 unit compared to the large pseudotetragonal distortion manifested in the extended Mo−O(1) distances along the *z* direction suggests that the splitting between the d_{xz} and d_{yz} orbitals will be insignificant relative to the separation between these two orbitals and d_{xy}. A small separation between d_{xz} and d_{yz} will permit the single electron of Mo^{5+} to occupy both orbitals, and therefore, the superexchange interactions will be considered by assuming partial population of d_{xz} and d_{yz} and zero occupation of d_{xy}. In the following discussion the electron can be assumed to occupy the d_{xz} orbital, leading to the interaction shown, or the d_{yz} orbital as indicated by brackets, leading to the coupling shown in parentheses.

The magnetic interaction along the *z* direction of the unit cell arises from a mixture of σ correlation between the empty d_{z^2} orbitals, π correlation between Mo $d_{yz}^{0(1)}$ and Nd t_{2g}^0, and π correlation between Mo $d_{xz}^{1(0)}$ and Nd t_{2g}^0. The first of these interactions would favor antiparallel alignment, the second would lead to antiferromagnetic (ferromagnetic) coupling, and the third would lead to ferromagnetic (antiferromagnetic) coupling; i.e., antiferromagnetic coupling results if the Mo d orbital is empty and ferromagnetic coupling if the orbital is half-filled. The ferromagnetic π exchange will be reinforced by a delocalization exchange between half-filled Mo orbitals and the empty Nd orbitals. Due to the near linearity of the Mo−O−Nd bonding in the *z* direction, this delocalization interaction will be significant.

The interaction in the *x* direction arises from a mixture of σ correlation between the empty $d_{x^2-y^2}$ orbitals, π correlation between the Mo d_{xz} (which statistically accommodates $^1/_2$ electron) and Nd t_{2g}^0, and π correlation between Mo d_{xy}^0 and Nd t_{2g}^0. The interaction in the *y* direction is the same as in the *x* direction. The large angular distortion, 162.7°, in this exchange pathway will greatly weaken any delocalization superexchange in the *xy* plane. These arguments lead us to conclude that the interactions in the *x* and *y* directions have $<^1/_2$ of the ferromagnetic component of the interaction in the *z* direction as a consequence of the Jahn−Teller distortion of the molybdenum oxide octahedron. The observed magnetic structure shows ferromagnetic coupling of nearest neighbors along the *z* direction of the unit cell and antiferromagnetic coupling in the *xy* plane. This suggests the splitting of the t_{2g} manifold of Mo^{5+} plays the key role in determining the magnetic structure.

(25) Goodenough, J. B. *Magnetism and the Chemical Bond*; Interscience Publishers: New York, 1963.
(26) Bertaut, E. F. *Acta Crystallogr.* **1968**, *A24*, 217.

The absence of either magnetic order or Jahn−Teller distortion in the other compounds studied suggests that these observations in Ba_2NdMoO_6 are dependent on the size mismatch between Ba^{2+} and the $NdMoO_6^{4-}$ framework. While bond valence sum analyses show that this is driven by the bonding requirements of Ba^{2+}, this distortion introduces the inequivalence in the oxide ion sublattice that permits the electronically driven distortion on cooling. Without such structural distortion already present, the electronic stability conferred by Jahn−Teller distortion is insufficient to induce a deformation of the structure, and thus, the cubic double perovskites remain perfectly geometrically frustrated. The complexities of this behavior indicate that interpretation of the magnetic properties of Mo^{5+} oxides may be more complex than has hitherto been assumed. We also note the degeneracy in the t_{2g} manifold is more common than in the e_g set, so the arguments we have developed here may apply to a large number of oxide phases containing 4d and 5d metals.

Conclusion

The compounds Ba_2LnMoO_6 (Ln = Nd, Sm, Eu, Gd, Dy, Er, Y, Yb) form cation-ordered perovskite phases. The tetragonal structural distortion observed for the two largest lanthanides is driven by the necessity of satisfying the bonding requirements of Ba^{2+}, which is too small to fit inside the central interstice of a theoretical cubic structure when Ln = Nd or Sm. All other compounds are cubic and show no evidence for a magnetic transition at temperatures down to 2 K, the lowest temperature accessed. The absence of magnetic order in the higher symmetry compounds arises from cancellation of magnetic coupling due to perfect geometrical magnetic frustration in these structures. The antiferromagnetic structure adopted by Ba_2NdMoO_6 is determined by the Jahn−Teller effect observed in the molybdenum coordination environment. This causes a splitting of the t_{2g} manifold, resulting in depopulation of the d_{xy} orbital, which leads to an enhanced ferromagnetic component of the magnetic superexchange interactions in the *z* direction and a magnetic structure containing chains of ferromagnetically coupled Nd^{3+} and Mo^{5+} aligned antiparallel to neighboring chains. This series thus shows that magnetic ordering is dependent on structural distortion from cubic symmetry and that the degenerate electronic state of Mo^{5+} can generate anisotropic magnetic coupling. These observations suggest that the Mo^{5+} cation may be a good candidate to use in the design of materials with unusual tailored magnetic properties.

Acknowledgment. E.J.C. is grateful to the Royal Society for the provision of a university research fellowship and a research grant to support this work. We are grateful to Dr. Ron Smith (ISIS) and Dr. Clemens Ritter and Dr. Paul Henry (ILL) for experimental assistance with neutron diffraction experiments and to both of these institutions for providing access to their facilities.

Supporting Information Available: Structural data for Ba_2NdMoO_6 and Ba_2SmMoO_6, structural parameters for cubic phases Ba_2LnMoO_6, and ac molar magnetic susceptibility data for Ba_2LnMoO_6. This material is available free of charge via the Internet at http://pubs.acs.org.

CM0602388